

Article

Fiber-Reinforced Sand-Fixing Board Based on the Concept of “Sand Control with Sand”: Experimental Design, Testing, and Application

Bosong Ding, Jianjun Cheng *, Duotian Xia, Xiao Wu, Li Gao, Benteng Ma, Dongsheng Li and Zhujie Lin

College of Water Resources and Architectural Engineering, Shihezi University, Shihezi 832003, China; dingbs0606@163.com (B.D.); xdt_xxl@shzu.edu.cn (D.X.); wx04520030@126.com (X.W.); gaoli03122@163.com (L.G.); mabt_shz@163.com (B.M.); dsli909@126.com (D.L.); 1932874230@163.com (Z.L.)

* Correspondence: chengdesign@126.com



Citation: Ding, B.; Cheng, J.; Xia, D.; Wu, X.; Gao, L.; Ma, B.; Li, D.; Lin, Z. Fiber-Reinforced Sand-Fixing Board Based on the Concept of “Sand Control with Sand”: Experimental Design, Testing, and Application. *Sustainability* **2021**, *13*, 10229. <https://doi.org/10.3390/su131810229>

Academic Editors:

Panagiotis Georgakis,
Efthimios Bothos, Babis Magoutas
and Michiel de Bok

Received: 3 August 2021

Accepted: 8 September 2021

Published: 13 September 2021

Publisher’s Note: MDPI stays neutral with regard to jurisdictional claims in published maps and institutional affiliations.



Copyright: © 2021 by the authors. Licensee MDPI, Basel, Switzerland. This article is an open access article distributed under the terms and conditions of the Creative Commons Attribution (CC BY) license (<https://creativecommons.org/licenses/by/4.0/>).

Abstract: Harsh conditions, such as the lack of raw materials and high transportation costs, impede the construction of desert railway sand control projects. Against this background, aeolian sand along the desert railway was used in a study on “sand control with sand.” According to the mechanical properties and durability tests, as well as field observations, the enhancement effect of fiber (cloth) on the performance of a sand-fixing board made of aeolian sand was analyzed. Based on the results, the mechanical strength of the sand-fixing board increased with increasing fiber content and length, and the maximum increase in compressive strength and flexural strength reached 2.15 and 0.59 times, respectively. The addition of fiber significantly improved the frost resistance, effectively reducing the mass loss rate of the board by an average of 60%. With increasing fiber content and length, the improvement effect of the freeze–thaw strength loss rate of the sand-fixing board first decreased and then increased. The results show that the performance of sand-fixing boards reached the engineering application standard under the reinforcement of the fiber (cloth), successfully establishing the concept of “sand control with sand.”

Keywords: sand control with sand; sand-fixing materials; fiber-reinforced sand-fixing board; sand barrier; wind-sand control engineering

1. Introduction

Land desertification threatens the survival of humans and affects social development. The desertified surface provides sufficient sources of sand for the wind-sand movement, forming wind-sand disasters under the action of wind, which threatens the safety of transportation, industry, agriculture, and communications. The commonly used sand-fixing technologies include engineering, chemical, and biological technologies [1–3]. The corresponding sand-fixing materials are concrete, polyethylene, wire mesh, wood, reed-based plant straw, and certain microbial sand-fixing materials. With the advancement of environmental protection projects, most of these materials cannot meet the current requirements for sand-fixing costs, energy conservation, and environmental protection [4]. In addition, most of the wind-sand control projects are located in remote areas with inconvenient transportation, resulting in a large consumption of labor and resources [5,6]. The cost of chemical sand-fixing materials is high [7], and long-term use will cause new environmental problems [8]. Plant species that are suitable for sand fixing are scarce, have long growth cycles, and can hardly adapt to the harsh environment of deserts, at least in the early growth stages. It is therefore of great significance to study and develop new sand-fixing materials in combination with specific wind-sand control projects.

Research on the development and use of new sand-fixing materials has achieved remarkable results in China and abroad. In recent years, domestic research has mainly focused on chemical sand fixing, such as polymer materials, organic–inorganic composite

materials, and modified waste plastic materials [9–13]. International researchers have conducted numerous studies on microbial soil modification [14–16], using microbial metabolic activities to induce or control a series of chemical reactions in the soil to improve the soil, thereby achieving sand fixation [17–19].

However, studies on the improvement and upgrading of traditional sand-fixing materials are scarce; this is especially the case for the use of desert aeolian sand resources for wind-sand control. The implementation of “sand control with sand” projects will greatly reduce the project costs, shorten the construction period, rationally use aeolian sand resources, and meet the requirements of sustainable development and environmental protection. However, studies showed that desert aeolian sand can replace traditional construction sand only to a certain extent [20–22]; the cement-based material of desert aeolian sand has a lower strength compared with cement mortar made of traditional construction sand and cannot meet the application standards of wind-sand control projects [23,24]. Therefore, to further explore the feasibility of applying aeolian sand-to-sand control projects, this study took the wind-sand disaster area along the Ejina–Hami railway as an example, used the abundant aeolian sand resources along the desert railway to obtain local materials, and adopted the desert aeolian sand to fully replace the traditional construction sand as the aggregate of cement-based materials. The overall performance of the sand-fixing material was improved by adding fibers [25]. Numerous studies have shown that fibers have a positive impact on the mechanical properties [26–28], durability [29,30], and failure mode [31] of concrete composites. In addition, research on finite element modeling and the numerical simulation of fiber-reinforced concrete is also underway [32].

Based on numerous indoor and field tests, the fiber-reinforced sand-fixing board with strong structure and low costs was prepared, whose strength and durability could meet the needs of practical projects and the requirements of environmental protection construction, achieving the purpose of “sand control with sand.” The research results showed the feasibility of the application of the improved aeolian sand material in the field of wind-sand control, promoted the research and development of new sand-fixing materials, and provided a new systematic method of “sand control with sand” for the configuration of sand control projects.

2. Overview of the Study Area

2.1. Regional Geographical Characteristics

The Ejina–Hami railway starts at Ejina Banner, Inner Mongolia Autonomous Region, in the east and ends at Hami, Xinjiang Uygur Autonomous Region, in the west. The geographic coordinates are $93^{\circ}35.97'$ – $101^{\circ}3.74'$ E and $41^{\circ}57.62'$ – $42^{\circ}44.95'$ N and the total length of the line is 644 km (Figure 1). The starting point is close to the Badain Jaran Desert and 95% of the road sections along the railway are in the Gobi Desert area. Under the action of the incoming wind, which intersects the line at a large angle, some sections of the railway have different forms of sand damage, such as sand accumulation at the rail, the foot of the subgrade slope, and the culverts (Figure 2a–c), requiring immediate action. The wind-blown sand section of the Xinjiang region is mainly distributed in the denuded hilly area of the North Tianshan Mountains and the local gullies in the piedmont alluvial inclined plain area. The surface is composed of fine round gravel soil and silty fine sand soil formed by diluvion, providing sand source conditions for the formation of sand damage. To ensure a clear railway line, it is necessary to carry out sand control projects along the line. However, the railway affected by wind-sand disasters is located in the uninhabited area of the Gobi Desert. The construction of sand control projects requires that the material is transported over long distances, increasing the project costs. Sufficient sand sources near the railway provide abundant, cheap, and convenient desert aeolian sand. In this context, based on the scientific concept of “sand control with sand,” the use of desert aeolian sand to replace sand and stone aggregates in ordinary concrete makes it possible to prepare new sand-resisting and sand-fixing materials.

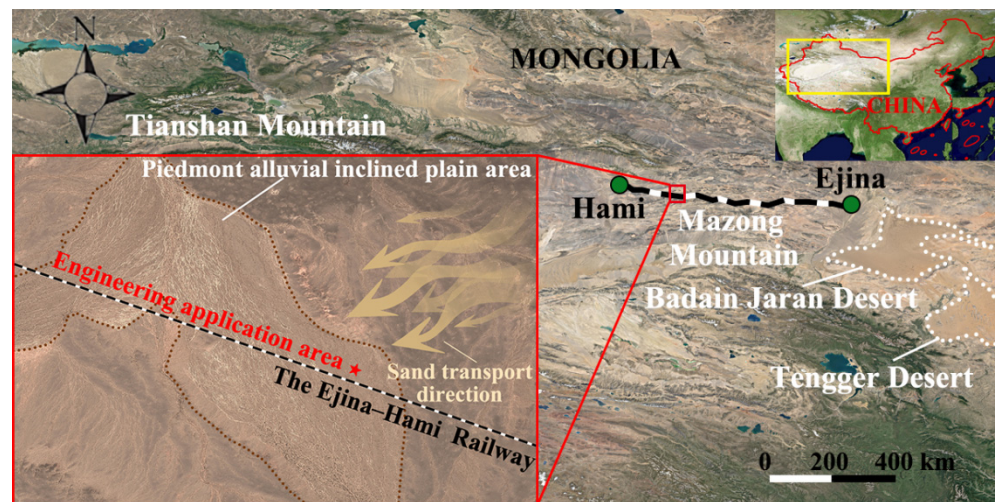


Figure 1. Geographical location of the Ejina–Hami railway line.

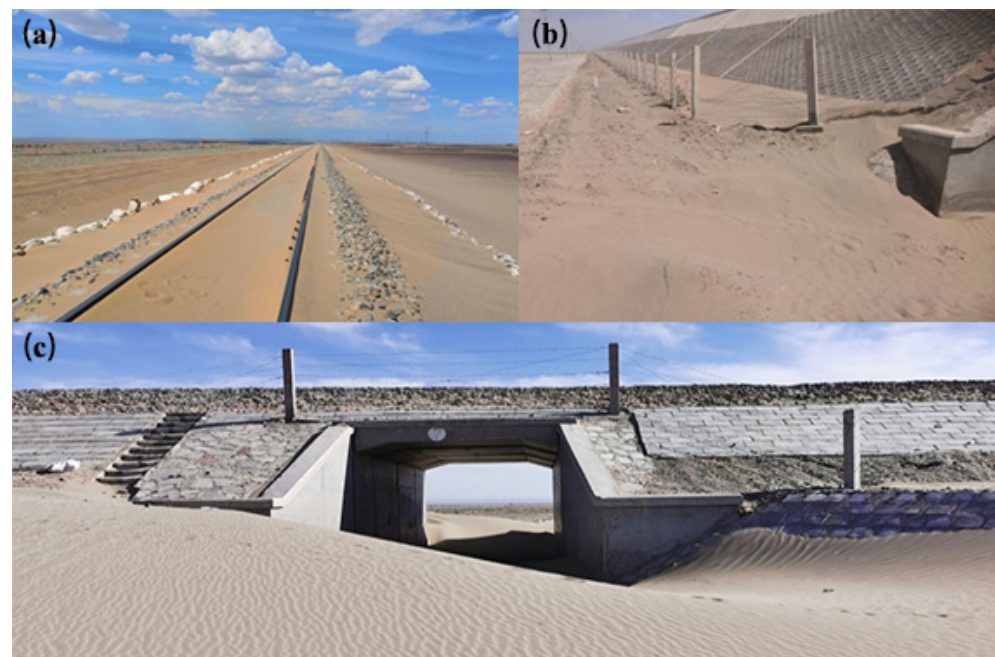


Figure 2. Sand damage along the Ejina–Hami railway: (a) accumulating sand in the orbit; (b) accumulating sand in the slope toe; (c) accumulating sand in the culvert.

2.2. Regional Wind Conditions

In addition to the sand source and micro-topography conditions, wind conditions that are greater than the wind speed of sand-driving also contribute to the formation of wind-sand disasters along the Ejina–Hami railway line. The study area is located in the piedmont alluvial inclined plain area; sand damage is serious in many gullies formed by the diluvium along the railway. To reveal the wind condition characteristics in this area, the latitude and longitude coordinates along the railway ($95^{\circ}54.42'$ E, $42^{\circ}24.68'$ N) were selected as the study area (corresponding to the later engineering application area). Using the atmospheric reanalysis of the global climate data (ERA5) as the data source, the 3-year wind data at a height of 10 m above the ground were obtained. Statistical analysis of these data revealed that the frequency distribution of spring and autumn wind directions in the region was relatively uniform, whereas the main wind direction in summer and winter was significantly different. The main wind direction in summer was SSW, whereas, in winter, it was NE and ENE. The average wind speed and the maximum wind speed in winter were

significantly higher than the average wind speed in summer. In general, the frequency of NE and ENE in this area throughout the year reached 22.52–25.30%, making it the dominant wind direction (Figure 3). The annual average wind speed was 4.48 m/s, with a maximum of 17.31 m/s (Figure 4). These conditions can facilitate wind-sand disasters.

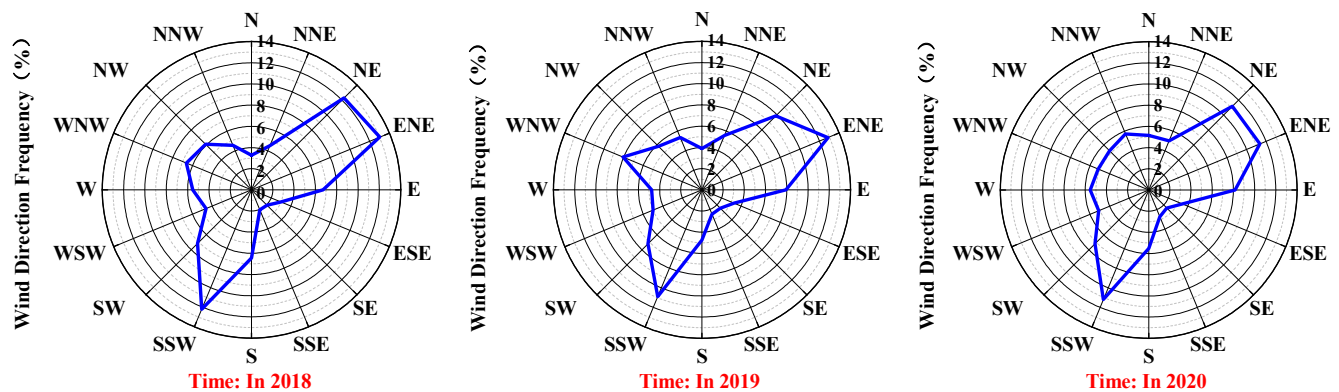


Figure 3. Wind direction frequency.

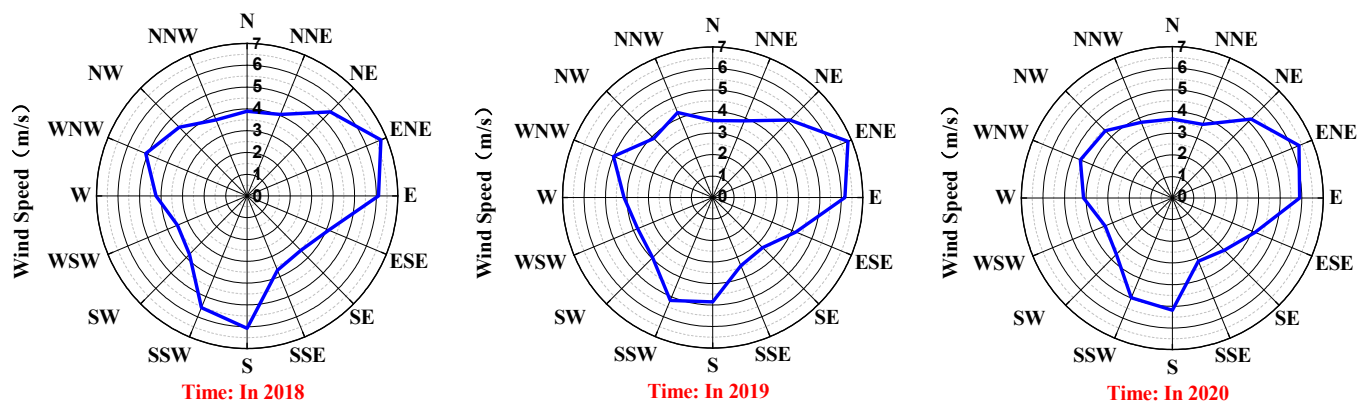


Figure 4. Wind speed.

The drift potential (DP) reveals the potential of sand transport in an area based on wind data. The drift potential is also called drift wind energy, which refers to the ability to transport sand in a certain direction within a certain period, as represented with vector unit (VU) values. The resultant direction and vector of the drift potential from 16 directions are termed the resultant drift direction (RDD) and the resultant drift potential (RDP), respectively. The equation for the drift potential was proposed by Fryberger (1979), as shown below:

$$q = u^2(u - u_t)t \quad (1)$$

where q denotes the drift potential (VU); u denotes the wind speed at a height of 10 m (m/s); u_t denotes the threshold wind velocity (m/s), i.e., the critical value of the wind speed that gradually increases until the surface sand particles begin to move from a stationary state, which is ≥ 5 m/s; t denotes the percentage (%) of the time the wind speed is ≥ 5 m/s during the total observation period.

The drift potential of each direction was calculated using the above equation and the drift potential was drawn (Figure 5). In 2018, 2019, and 2020, the drift potential values were 79, 67, and 53 VU, the resultant drift potentials were 24, 30, and 22 VU, and the resultant drift directions were 269° , 258° , and 266° , respectively. According to the wind energy environment classification method of Fryberger et al. (1979), the wind energy environment was divided into high-energy (DP > 400), medium-energy (DP between 200 and 400), and low-energy (DP < 200) environments.

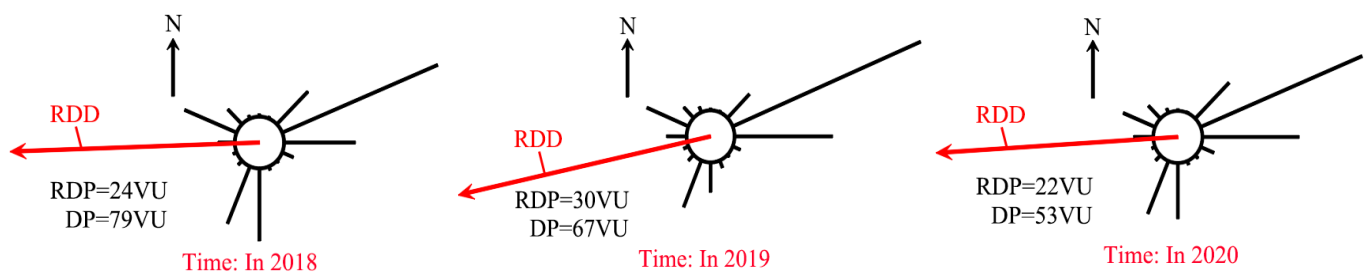


Figure 5. Drift potential.

Although the study area is located in a low-energy area, according to the wind speed statistics for the past 3 years, the probability that the overall wind speed exceeded the threshold wind velocity (5 m/s) was 44.41%, mainly in the NE and ENE directions, and the maximum wind speed could reach 17.31 m/s. This indicates that the area showed the characteristics of intermittent drift, and the drift direction was stable. The average and maximum wind speed values in each direction are shown in Figure 6. Although the annual drift potential was small, the wind conditions greater than the threshold wind velocity were concentrated in time. Thus, aeolian sand accumulation along the railway was possible, and the construction of wind-sand control projects along the line is required.

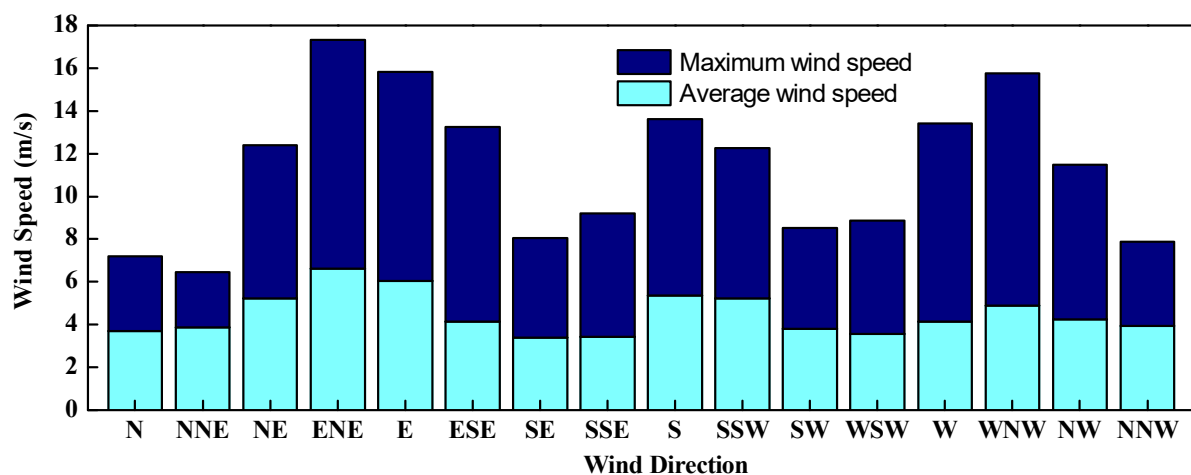


Figure 6. Average and maximum wind speed values.

3. Materials and Methods

3.1. Sand-Fixing Board Material

To achieve the project goal of “sand control with sand,” aeolian sand was selected as the raw material for sand fixation and sand barrier production. On this basis, fiber (cloth) materials were added to improve the mechanical properties of the sand barrier boards. The materials required for the production of sand barrier boards include aeolian sand, ordinary cement, fiber, and fiber cloth.

The aeolian sand was taken from the accumulated sand in the Ejina–Hami railway sections with more severe sand damage (Figure 7). The main chemical components of aeolian sand are SiO_2 , Al_2O_3 , CaO , and MgO , and the particle size distribution is relatively uniform. The characteristics of the aeolian sand under the electron microscope are shown in Figure 8. At $40\times$ magnification, it can be seen that the particle size of aeolian sand mainly ranges from 60–250 μm . At $1600\times$ magnification, the apparent characteristics of single sand grains can be observed, which shows that its surface features are uneven, with obvious abrasion marks, edges, and smoothed corners. The particle size distribution of the sand sample was tested using a laser particle size analyzer (Figure 9). The most common and average particle size values of the desert aeolian sand used in the test were 161.4 and 139.6

μm , respectively, characterizing extremely fine sand, and the particle size distribution was relatively concentrated. Compared with ordinary construction sand, the relative specific surface area of desert aeolian sand was larger, the gap between particles was greater, and the bulk density was lower, resulting in a higher porosity. The basic physical properties are shown in Table 1.

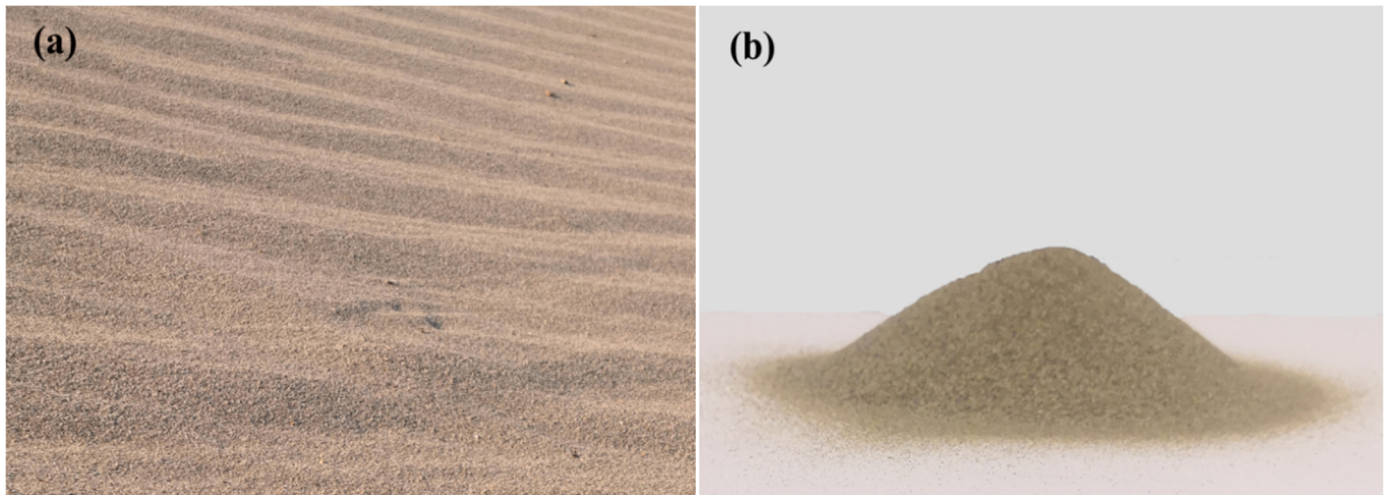


Figure 7. Pictures of desert aeolian sand: (a) natural form; (b) accumulation form.

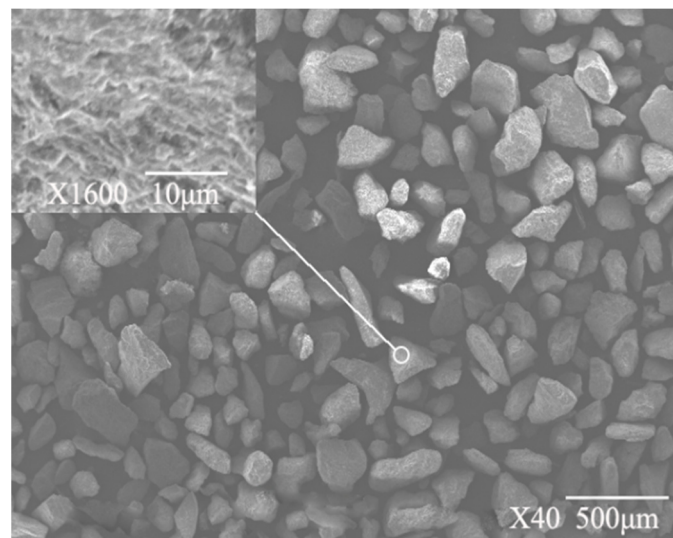


Figure 8. Scanning electron microscope image of desert aeolian sand.

Table 1. Physical properties of desert aeolian sand.

Fineness Modulus	Compact Bulk Density (kg/m^3)	Loose Bulk Density (kg/m^3)	Apparent Density (kg/m^3)	Porosity (%)	Mud Content (%)
0.252	1469	1307	2665	44.87	3.6

P.O-42.5-grade ordinary silicate cement was used in accordance with Chinese national standards. Its physical and mechanical properties are shown in Table 2.

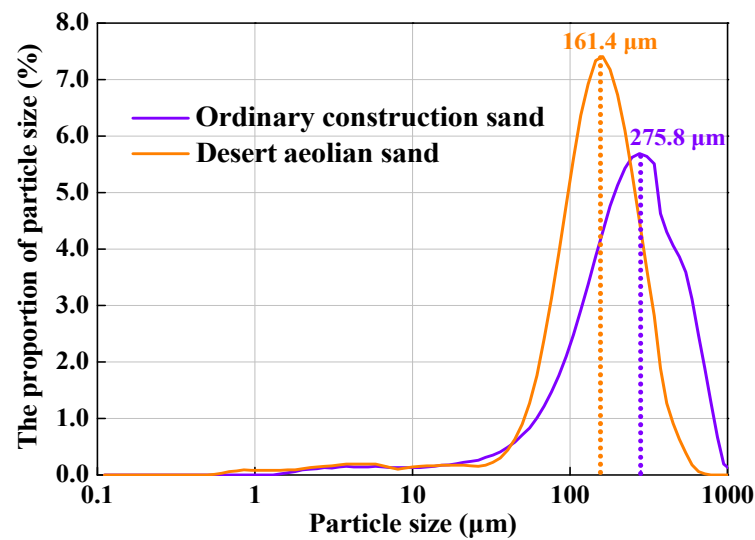


Figure 9. Particle size distribution curve of desert aeolian sand.

Table 2. Physical and mechanical properties of the cement used in this study.

Test Items	Setting Time (min)		Flexural Strength (MPa)		Compressive Strength (MPa)	
	Initial Set	Final Set	3 Days	28 Days	3 Days	28 Days
Measured value	134	218	6.5	10.3	29.2	52.9
Standard deviation	4.32	8.29	0.22	0.36	1.10	1.51

Polypropylene fiber and glass fiber mesh cloth were used to enhance the performance of the sand-fixing board. Polypropylene fiber is shown in Figure 10a and the specific physical parameters are shown in Table 3. The glass fiber mesh cloth is shown in Figure 10b and the specific physical parameters are shown in Table 4.

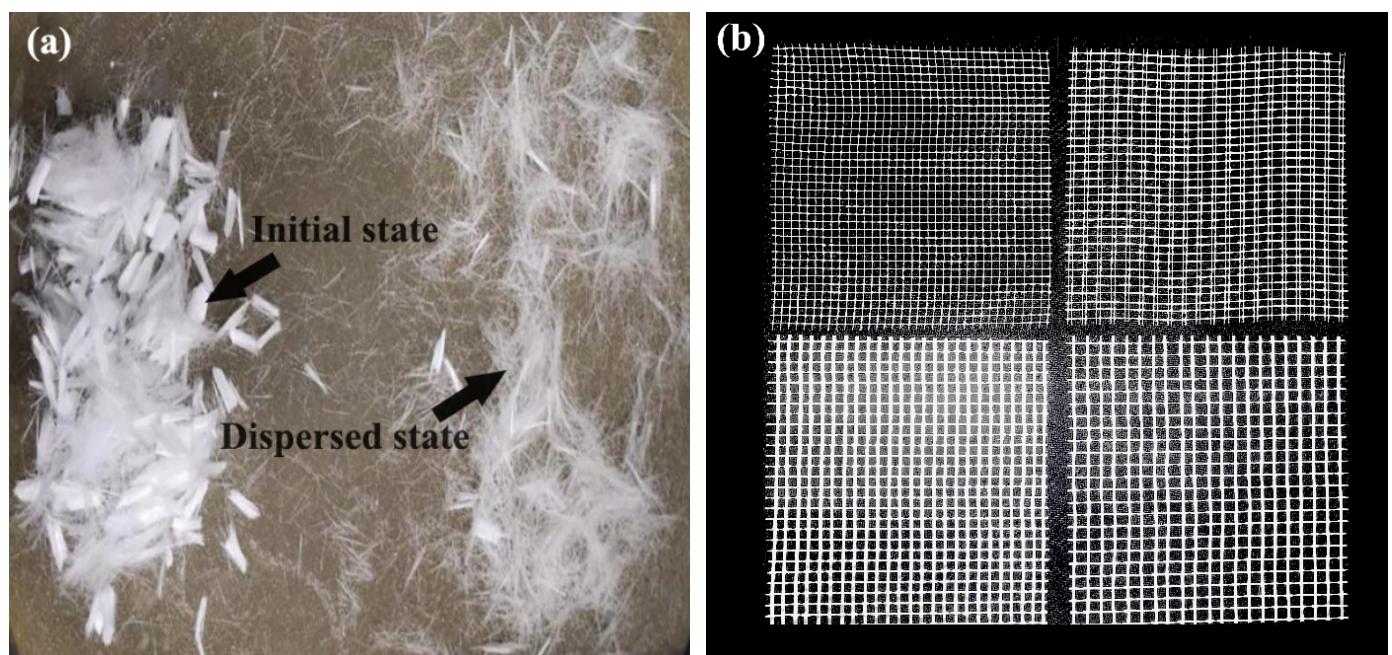


Figure 10. Morphology of different fibers: (a) polypropylene fiber; (b) glass fiber mesh cloth.

Table 3. Main physical properties of polypropylene fiber.

Fiber Name	Linear Density (μm)	Tensile Strength (MPa)	Elongation at Break (%)	Modulus (Elongation of 15%) (MPa)	Melting Point ($^{\circ}\text{C}$)
Polypropylene fiber	19.2	556.9	29.8	6822.3	160

Table 4. Main physical properties of glass fiber mesh cloth.

Unit Area (g/m^2)	Pore Size (Mesh \times Mesh)	Longitudinal Tensile Strength (N/50 mm)	Transverse Tensile Strength (N/50 mm)	Longitudinal Fracture Strain (%)	Transverse Fracture Strain (%)	Binder Content (%)
46	3 \times 3	452	461	3.8	3.9	13.5
78	5 \times 5	572	606	3.6	3.9	13.4
121	5 \times 5	751	798	3.5	3.7	13.8
135	5 \times 5	896	968	3.8	3.9	13.5
162	5 \times 5	1221	1765	3.6	3.5	13.8

3.2. Experimental Design and Testing

Based on the above raw materials, a mix ratio test was conducted to select the most suitable mix ratio. Based on this, combined with the comparison test of the mechanical property and durability of the sand-fixing board with different fiber contents, the performance of the sand-fixing board was further improved.

Combining the requirements of engineering use, the size of the sand-fixing board was $1000 \times 300 \times 25 \text{ mm}^3$ as a rectangular board specimen, which was used for determining the mechanics and durability. The cement mortar strength standard M10, which is commonly used in construction, was applied. According to the Chinese standard “GBT 30100-2013 Test Methods for Building Wallboard,” the specimens without fiber were used as the reference group, and the fiber-reinforced specimens were used as the comparison group. The fiber content and length were changed while ensuring other factors remained unchanged (Table 5). The sand:binder ratio was 3:1, and the water:binder ratio was 0.9.

Table 5. Quality mix ratio of the test scheme.

Test Number	Desert Sand	Cement	Fiber	Fiber Length(mm)	Water: Binder Ratio
JZ0	3	1	0	0	0.9
DB1	3	1	0.0025	9	0.9
DB2	3	1	0.0025	12	0.9
DB3	3	1	0.0025	15	0.9
DB4	3	1	0.0025	19	0.9
DB5	3	1	0.005	9	0.9
DB6	3	1	0.005	12	0.9
DB7	3	1	0.005	15	0.9
DB8	3	1	0.005	19	0.9

After determining the scheme of the test mix ratio, the samples were prepared. During preparation, we weighed each material and then poured the desert sand and the cement into the mixer, followed by thorough mixing. The short fibers were mixed into the water for dispersion. Subsequently, the dispersed short fibers and water were mixed with desert sand and cement for 3 min. Finally, the mixed material was placed into the mold and allowed to form the sand-fixing board. The entire process did not exceed 30 min. Combined with the practical application of the sand-fixing board, the mechanics and durability of the board were investigated.

3.2.1. Mechanical Properties

Sand-fixing boards mainly bear the wind pressure generated by the sand-carrying wind and the impact pressure generated by the impact of sand particles, as well as the hoisting stress of the board during transportation and installation. If the board itself is not strong enough, it will be damaged and broken under force. The compressive strength and flexural strength of the board were tested using a testing machine (Figure 11).

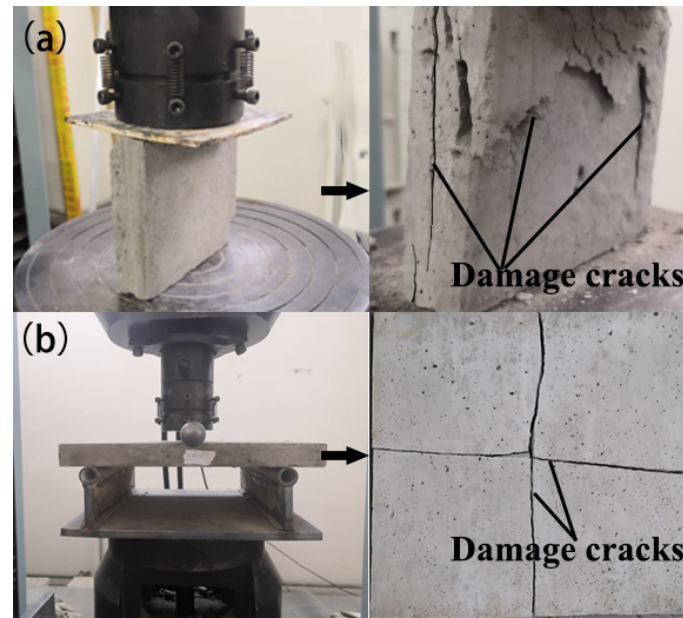


Figure 11. Mechanical strength tests: (a) compressive strength test; (b) flexural strength test.

Compressive Strength

A specimen with a size of $100 \times 100 \times 25 \text{ mm}^3$ was placed on the bearing plate of the testing machine; the axis of the specimen coincided with the pressure center of the bearing plate of the testing machine. The specimen was then loaded at a speed of $0.05\text{--}0.10 \text{ MPa/s}$ until it was damaged, and the maximum damage load P was recorded. The compressive strength of the specimen was calculated according to the following equation:

$$R = \frac{P}{L \times B} \quad (2)$$

where R denotes the compressive strength of the specimen (MPa), P denotes the failure load (N), L denotes the compression face length of the specimen under load (mm), and B is the compression face width of the specimen (mm).

The test results were calculated and evaluated based on the average value of the compressive strength of three specimens, and the results were rounded to 0.01 MPa. If the difference between the compressive strength of one of the specimens and the average value of three specimens exceeded 20%, the compressive strength value was calculated as the average value of the compressive strength of the other two specimens. If the test value of two specimens exceeded the standard, the test result was invalid, and resampling was performed.

Flexural Strength

The specimen with a size of $250 \times 250 \times 25 \text{ mm}^3$ face up was placed on the support. The diameter of the support and the compression bar was 20–30 mm so that the center line of the specimen and the loading rod were coincident; the support span was 215 mm. The loading speed was $20 \pm 5 \text{ N/s}$ until failure. Then, the failure load was read and the width of the fracture and the thickness of the two ends of the specimen were measured. A

second bending resistance in the vertical direction was applied and the measurement was repeated. The unidirectional flexural strength of the specimen was calculated as follows:

$$S = \frac{3pl}{2be^2} \quad (3)$$

where S denotes the flexural strength of the specimen (MPa), p is the failure load (N), l denotes the support moment of the specimen (mm), b represents the section width of the specimen (mm), and e denotes the section thickness of the specimen (mm).

The flexural strength of the specimen was the average of the test results in two directions, and the results were rounded to 0.01 MPa. The board flexural strength was expressed as the average value of four specimens, where the results were rounded to 0.01 MPa.

3.2.2. Durability

In Xinjiang and northern Inner Mongolia, the winter is long and cold. Low temperature and repeated freeze–thaw cycles will seriously affect the durability of the sand-fixing board and shorten its service lifespan, making it necessary to verify the frost resistance of the sand-fixing board.

Frost resistance is mainly evaluated in terms of three aspects: appearance, mass loss rate, and freeze–thaw strength loss rate. The mass loss rate of each specimen was calculated according to Equation (4), and the freeze–thaw strength loss rate was calculated according to Equation (5):

$$K_m = \frac{m_1 - m_2}{m_1} \quad (4)$$

where K_m denotes the mass loss rate (%), m_1 denotes the mass before the freeze–thaw (kg), and m_2 denotes the mass after the freeze–thaw (kg);

$$K_R = \frac{R - R_1}{R} \times 100 \quad (5)$$

where K_R denotes the strength loss rate (%), R is the average compressive strength of the specimen in the natural state (MPa), and R_1 is the average compressive strength of the frozen and thawed specimen (MPa).

The mass loss rate and freeze–thaw strength loss rate of the board were expressed as the average value of three specimens, where the results were rounded to 0.01%.

4. Results and Discussion

According to the data obtained from the indoor test using the determined mix ratio scheme, the relationship curves for the compressive strength, flexural strength, mass loss rate, freeze–thaw strength loss rate, and fiber content and length were plotted.

4.1. Analysis of Mechanical Properties

The compressive strength and flexural strength of the sand-fixing board are shown in Table 6, and the relationship between the compressive strength, flexural strength, and fiber content and length is given in Figure 12.

Table 6. Test results.

Test Number	Compressive Strength (MPa)						Flexural Strength (MPa)					
	Measured Value			Standard Deviation			Measured Value			Standard Deviation		
	3 Days	7 Days	28 Days	3 Days	7 Days	28 Days	3 Days	7 Days	28 Days	3 Days	7 Days	28 Days
JZ0	4.34	5.86	6.34	0.52	0.84	1.03	1.33	1.80	2.03	0.19	0.24	0.19
DB1	6.40	7.64	11.78	1.09	1.72	3.90	1.43	1.89	2.49	0.10	0.25	0.11
DB2	5.10	7.91	12.16	0.73	0.44	0.86	1.49	2.03	2.67	0.05	0.08	0.12
DB3	6.03	8.33	13.82	0.54	1.03	0.78	1.66	2.23	2.9	0.10	0.51	0.21
DB4	5.30	9.02	14.58	0.22	0.71	3.43	1.92	2.25	3.12	0.14	0.22	0.39
DB5	5.60	7.67	12.14	0.65	0.52	0.24	1.89	1.96	2.67	0.18	0.07	0.07
DB6	5.23	7.94	12.49	0.59	2.17	2.08	1.73	2.11	2.69	0.16	0.06	0.12
DB7	5.11	8.45	14.40	0.62	0.89	2.93	1.54	2.34	2.91	0.15	0.18	0.41
DB8	6.46	9.30	20.03	0.79	0.51	1.78	2.03	2.35	3.22	0.18	0.27	0.47

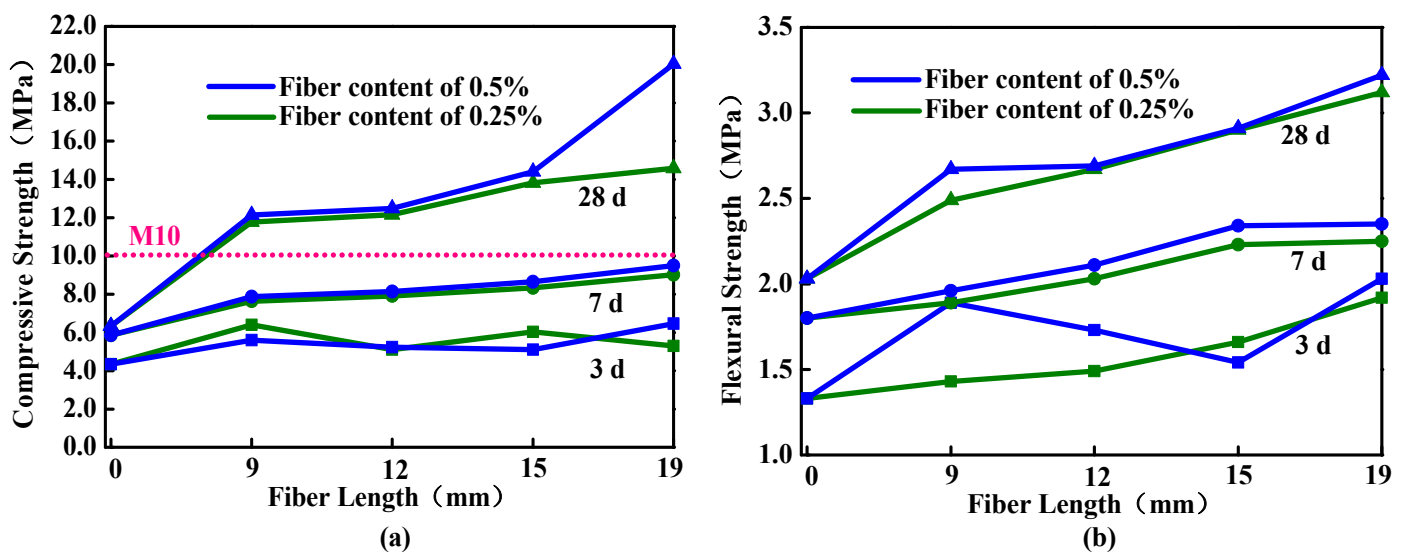


Figure 12. Relationship between the mechanical strength and the fiber content and length: (a) compressive strength; (b) flexural strength.

Based on Figure 12, with increasing fiber content, the overall strength of the sand-fixing board differed between the different stages. At 3 d, different fiber contents had little effect on the overall strength of the board. At this time, the mortar aggregate played a leading role in the overall strength of the board. At 7 d, the role of the fiber became obvious; the fiber content was positively correlated with the overall strength of the board, which was observed until 28 d. An increase in fiber length had no impact on the strength of the sand-fixing board at 3 d. However, the overall strength was increased at 7 d. At 28 d, the strength increased considerably with increasing fiber length. When the fiber length reached 19 mm, the compressive and flexural strengths of the board increased most significantly. In the reference group without fiber reinforcement, the compressive strength at 28 d did not reach M10, in contrast with the control group.

According to the test data, the regression function curve of the mechanical strength as a function of the fiber content and length of the sand-fixing board was obtained via fitting (Figure 13).

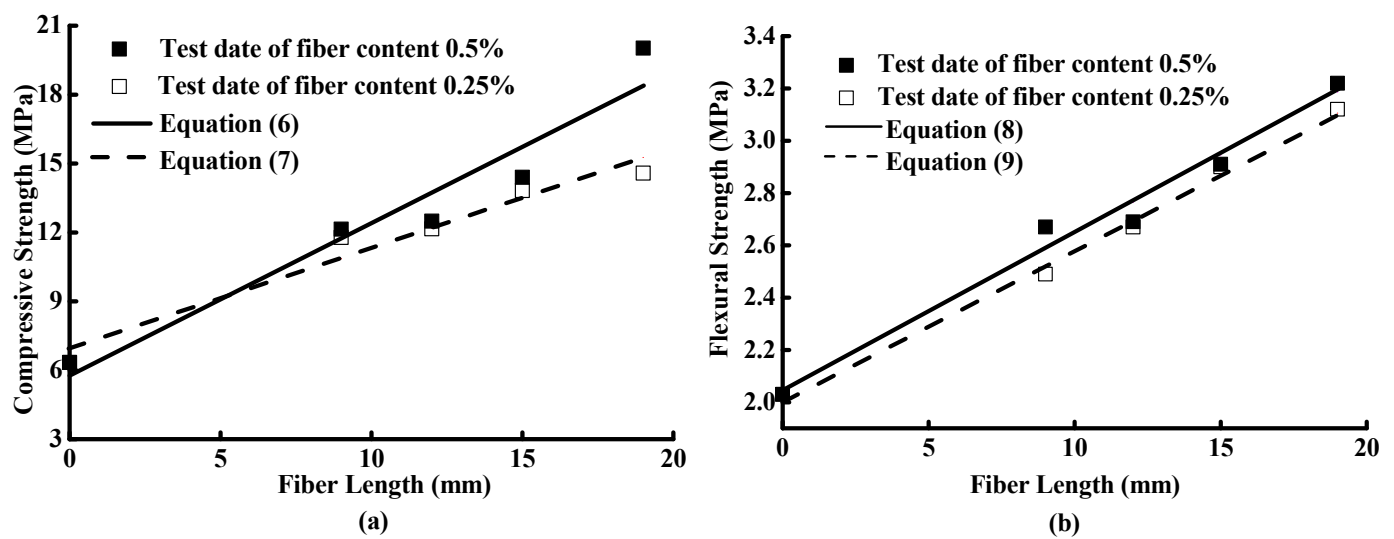


Figure 13. Regression function curves of mechanical strength of the fiber-reinforced sand-fixing board: (a) compressive strength; (b) flexural strength.

When the fiber content was 0.5%, the relationship between the compressive strength (R) and the fiber length (L_f) could be expressed using Equation (6):

$$R = 0.6617L_f + 5.8013, R^2 = 0.9327 \quad (6)$$

When the fiber content was 0.25%, the relationship between the compressive strength (R) and the fiber length (L_f) could be expressed using Equation (7):

$$R = 0.4407L_f + 6.8885, R^2 = 0.9587 \quad (7)$$

When the fiber content was 0.5%, the relationship between the flexural strength (S) and the fiber length (L_f) could be expressed using Equation (8):

$$S = 0.0603L_f + 2.0408, R^2 = 0.9797 \quad (8)$$

When the fiber content was 0.25%, the relationship between the flexural strength (S) and the fiber length (L_f) could be expressed using Equation (9):

$$S = 0.0579L_f + 2.0055, R^2 = 0.9946 \quad (9)$$

Based on the regression function obtained via fitting, the variation law of mechanical strength of the sand-fixing board increased linearly with fiber length, providing a reference for relevant studies.

Based on this, it could be concluded that the mechanical strength of the sand-fixing board had different degrees of improvement with the addition of fiber. With the increase in the fiber content and length, the overall strength of the board increased. When the fiber content was 0.5% and the fiber length was 19 mm, the compressive strength of the sand-fixing board reached 20.03 MPa and the flexural strength reached 3.22 MPa at 28 d. Compared with the control group, the compressive and flexural strengths increased by 2.15 and 0.59 times, respectively. Moreover, changing the fiber length had a more obvious effect on the board strength.

4.2. Durability Analysis

The appearance of the fiber-reinforced sand-fixing board with 0, 25, 50, and 75 freeze-thaw cycles is shown in Figure 14. The effect of freeze-thaw damage with or without fiber reinforcement is shown in Figure 15. The test results of the mass loss rate and

freeze–thaw strength loss rate are summarized in Table 7. The relationship between the mass loss rate, freeze–thaw strength loss rate, and fiber content and length was plotted (Figures 16 and 17).

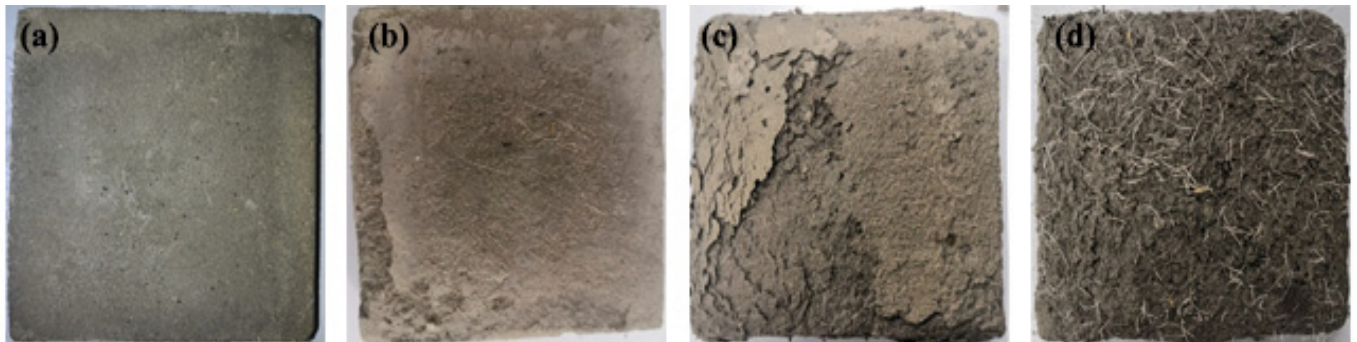


Figure 14. Morphology of a specimen after selected numbers of freeze–thaw cycles: (a) 0 freeze–thaw cycles; (b) 25 freeze–thaw cycles; (c) 50 freeze–thaw cycles; (d) 75 freeze–thaw cycles.

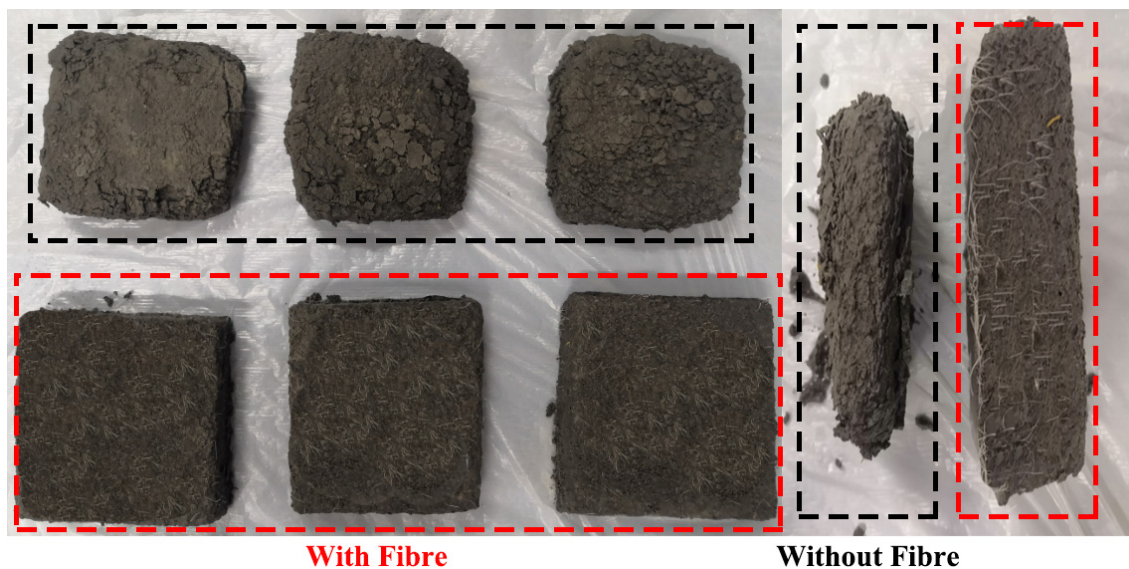


Figure 15. Freeze–thaw damage with and without fiber.

Table 7. Results of the freeze–thaw cycle test of the sand-fixing board.

Test Number	Mass Loss Rate (%)			Freeze–Thaw Strength Loss Rate (%)		
	25 Cycles	50 Cycles	75 Cycles	25 Cycles	50 Cycles	75 Cycles
JZ0	1.69	12.43	63.60	15.00	49.71	78.64
DB1	0.33	1.25	4.43	9.58	41.01	73.40
DB2	0.23	2.20	2.85	8.41	42.96	65.55
DB3	0.42	2.65	6.9	13.42	45.69	67.72
DB4	0.38	2.93	3.35	13.88	45.94	65.50
DB5	0.63	1.95	2.84	6.09	44.36	59.95
DB6	1.03	2.99	3.83	7.12	39.40	60.44
DB7	0.96	3.33	2.90	10.82	46.84	63.98
DB8	1.20	3.79	3.18	14.69	45.72	68.27

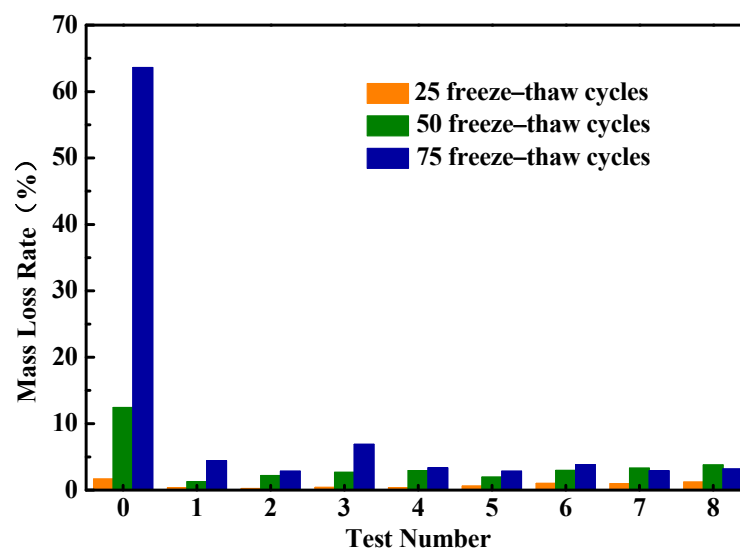


Figure 16. Statistical chart of mass loss rate of each group.

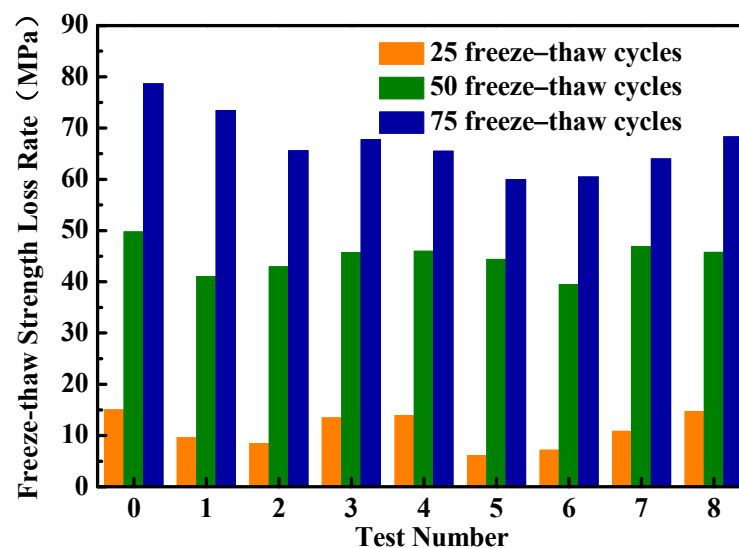


Figure 17. Statistical chart of freeze-thaw strength loss rate of each group.

As seen in Figures 14 and 15, as the number of freeze-thaw cycles increases, the apparent morphological damage of the specimens gradually increased. With 25 freeze-thaw cycles, the surface mortar at the corners of the specimens fell off, and the slag on the surface was uneven and rough, but the overall performance was not considerably affected. At this time, freezing damage occurred. With 50 freeze-thaw cycles, the surface mortar of the specimen fell off over a large area, and the mass loss increased significantly. At this time, the overall performance was greatly affected. With 75 freeze-thaw cycles, the mortar on the surface of the specimen was completely peeled off, the internal fibers were completely exposed, and the surface was soft. There were obvious traces of cracks and pores inside the structure, and the thickness of the specimen decreased. At this time, the freezing damage was significant.

Based on Figure 16, after adding the fiber, the integrity of the board was improved to varying degrees, and the mass loss caused by the freezing damage was reduced. The maximum mass loss rate of different freeze-thaw cycles was always the reference. With 25 freeze-thaw cycles, the board mass loss rate did not decrease significantly with the addition of fiber. At this time, the fiber did not significantly improve the frost resistance of the board. With 50 freeze-thaw cycles, the positive effect of the fiber started to become

obvious. It appeared that the mass loss rate of the board showed an obvious decreasing trend after adding the fiber. With 75 freeze–thaw cycles, the addition of fiber greatly reduced the mass loss rate, and the mass loss rate of most comparison groups did not exceed 5%. Compared with the reference group, the mass loss rate could be reduced by more than 60%.

As seen in Figure 17, the freeze–thaw strength loss rate of the specimen improved to varying degrees after the addition of fiber. With the increase of fiber content and length, the freeze–thaw strength loss rate of the specimen first decreased and then increased. This was because excessive fiber addition resulted in more pores. After several freeze–thaw cycles, the fiber, moisture, and other elements in the specimen underwent frost heave, which caused the main structure of the specimen to be destroyed from the inside. At this time, adding too much fiber or increasing its length might be counterproductive.

The results show that the morphology of surface damage of the sand-fixing board increased gradually with the increase in the number of freeze–thaw cycles. With more freeze–thaw cycles, the more obvious the improvement of the board frost resistance after the fiber addition. At 75 cycles, the mass loss rate of the board was reduced by more than 60%. After adding the fiber, the freeze–thaw strength loss rate of the board was improved, and with the increase of fiber content and length, the strength loss rate first decreased and then increased. In general, after adding fiber to improve the sand-fixing board, the integrity of the sand-fixing board was still intact after 25 freeze–thaw cycles, the mass loss rate did not exceed 1.5%, and the freeze–thaw strength loss rate did not exceed 15%.

4.3. Mechanism Analysis

The cement-based materials showed numerous micro-cracks. Because the particles of desert sand are considerably smaller than those of ordinary building sand, the micro-cracks in the desert sand cement-based materials were numerous. Under the action of an external force, these micro-cracks gradually expanded to form macro-cracks, resulting in material damage. The polypropylene fiber combined with desert sand cement-based materials, where its rough surface provided a strong adhesion stress. Adding an appropriate amount of polypropylene fiber can control the displacement of the crystalline structure in cement-based materials, and the cracking was blocked when it extended to adjacent fibers, thereby preventing the propagation of micro-cracks.

Polypropylene fiber has a polymer macromolecular structure. When the temperature decreases, the shrinkage resistance of glassy and crystalline macromolecules compensates for the thermal expansion and cold shrinkage characteristics of cement-based materials. In addition, numerous fibers, which were evenly distributed throughout the cement-based material, played a role in shunting and screening and reduced the water separation on the material surface; thus, it reduced the pore content with an internal diameter of 50–100 nm and greatly improved the impermeability, which was also conducive to the freeze–thaw resistance of the material.

5. Engineering Applications

According to the above indoor tests on the performance of the sand-fixing board, the optimal mix ratio (Table 8) was selected for field production and the construction process was optimized to solve the issues that were encountered during construction. After application to the damaged section of the Ejina–Hami railway line in the form of a checkerboard sand barrier, the near-surface wind speed at the project point was measured and the sand accumulation in the grid was observed.

Table 8. The mix ratio of the project construction.

Desert Aeolian Sand (kg/m ³)	Cement (kg/m ³)	Fiber Content (kg/m ³)	Fiber Length (mm)	Water (kg/m ³)	Sand: Binder Ratio	Water: Binder Ratio
1338.9	446.3	2.23	19	401.7	3:1	0.9

5.1. Construction Technology

The construction quality determines the overall quality of a project. Excellent construction technology is the basis for improving construction quality. The above-mentioned mix ratio was selected for batch pilot production of boards in the field, and the construction technology was continuously improved by discovering and solving problems during the construction process. Combined with the practical situation, the following problems were found:

- (1) Through field construction, the premature removal of molds under natural curing conditions resulted in too rapid water loss inside the board, inadequate hydration reaction, and a large number of early cracks. Given this, by delaying the demolding time and adopting the method of film curing, as shown in Figure 18, cracking could be significantly minimized.
- (2) The large-scale machinery used in the batch production of sand-fixing boards could not reach the same level of accuracy as that obtained in the laboratory, resulting in an uneven dispersion and agglomeration of fibers when directly mixed and stirred with aeolian sand cement-based materials. To keep the costs low, the fibers could be mixed and dispersed in water (Figure 19).

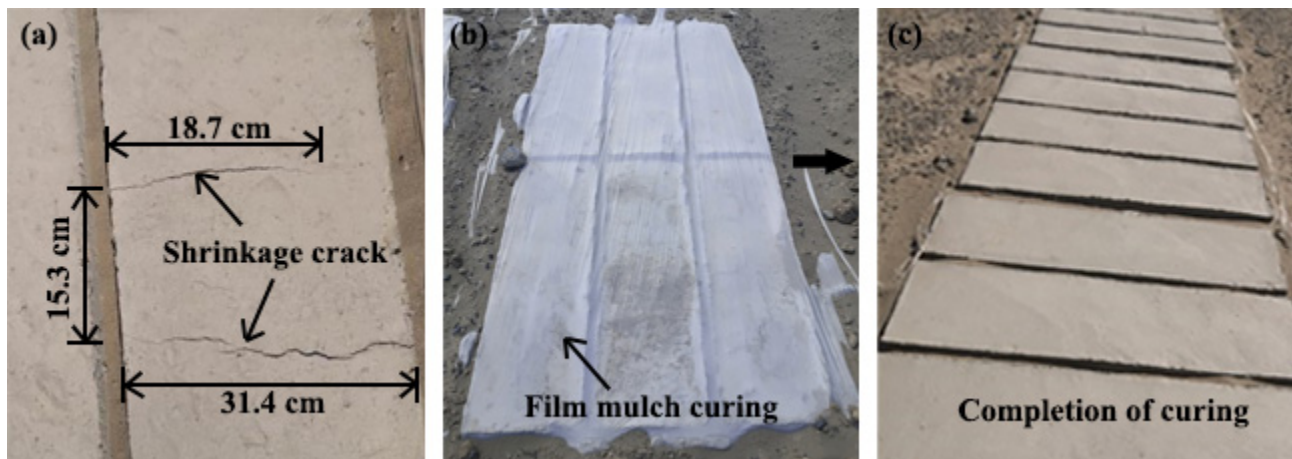


Figure 18. Pictures of the board before and after minimizing early cracking: (a) before improvement; (b) film curing; (c) after improvement.

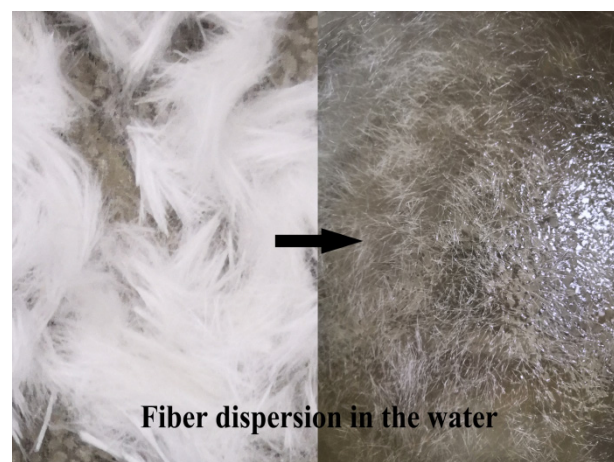


Figure 19. Fiber dispersion effect of fibers in water.

The above construction problems were solved, and the following construction techniques with strong practicability and simple operation were summarized as follows:

- (1) **Weighing:** Determine and weigh the dosage of each component of the sand-fixing board. The weighing accuracy should meet the requirements of $\pm 1\%$ for desert aeolian sand and $\pm 0.5\%$ for water, cement, fiber, etc.
- (2) **Feeding sequence:** To ensure that the fibers are uniformly dispersed and not agglomerated during the mixing process, other materials are first mixed and, subsequently, the fibers and water are added. The fiber-dispersing machine could be used for longer fibers.
- (3) **Stirring:** It is advisable to use a mixer, and the mixing amount should be 50 to 80% of the specified capacity of the mixer. Manual mixing could also be used on a steel plate or another non-absorbent platform. The plate and shovel surfaces are first wetted with a cloth, and various materials are added, followed by the addition of water for wet-mixing. During stirring, a shovel is used for mixing. The mixing time should not be less than 3 min.
- (4) **Die filling:** Small holes should be reserved at four corners of the mold bottom, and fixed piles, such as steel bars or bamboo poles, should be inserted to connect after sheet forming. Immediately, the die is filled in. The time interval should not exceed 15 min. The mold is filled as densely as possible, compacted, and flattened.
- (5) **Curing and splicing:** After die filling, the upper part must be covered with a film for curing. After 3 days of curing, the mold should be removed to take out the fixed pile. After reaching 70% of the design strength, the adjacent board should be assembled and spliced with iron wires for sand control projects, as shown in Figure 20.

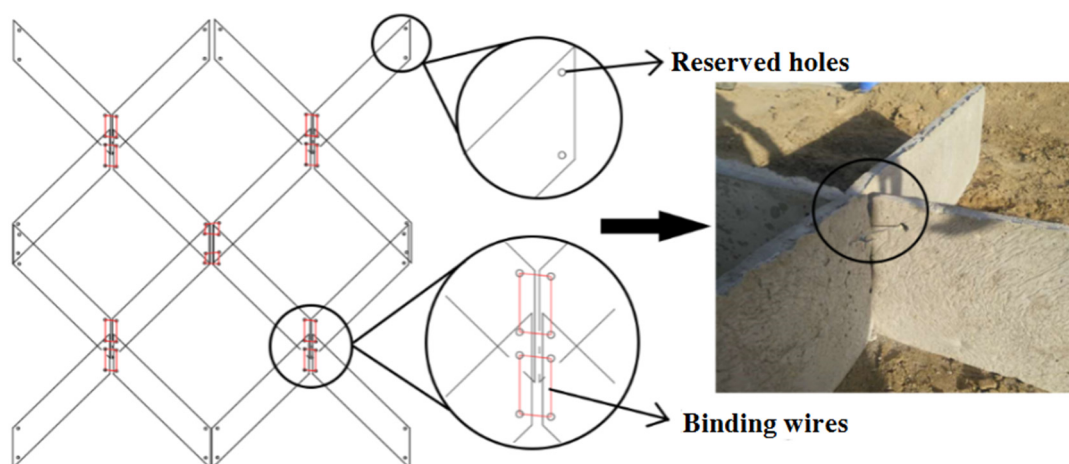


Figure 20. Details of board splicing.

5.2. Project Effectiveness

Combining a large number of preliminary tests and the above-mentioned construction technology, the fiber-reinforced sand-fixing board studied in this article was applied to the K1254~K1259 section of the Ejina–Hami railway in the form of a checkerboard sand barrier, as shown in Figure 21. Local materials were used in this project to save on raw materials and transportation costs. The sand barrier was structurally strong, which effectively increased the surface roughness and played an important role in sand fixation.



Figure 21. Checkerboard sand barriers along the Ejina-Hami railway line.

To verify the functionality of the checkerboard sand barrier, portable wind meters were used to conduct near-surface wind speed tests inside and outside the sand barrier grids (Figure 22). A wind meter was set outside the grid to measure the initial wind speed, and wind meters were set at uniform intervals inside the grid along the wind direction. The height of each wind meter was the same as the upper edge of the sand-fixing board, that is, 30 cm above the ground. The wind speed was measured, and the results are shown in Figure 23.

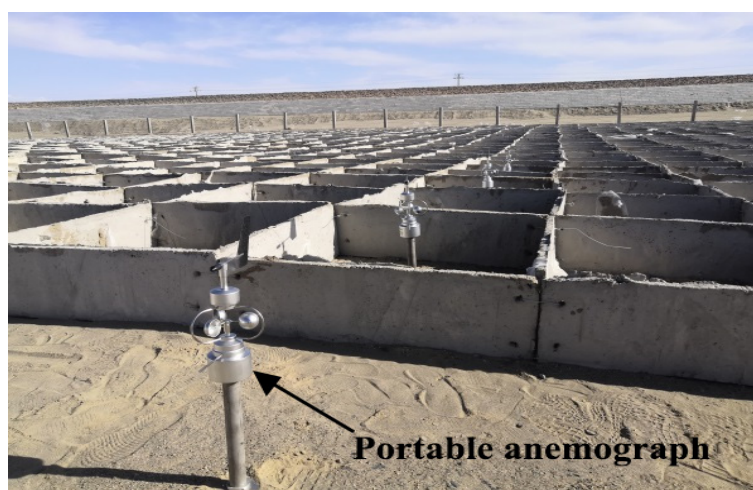


Figure 22. Layout of the portable wind meters.

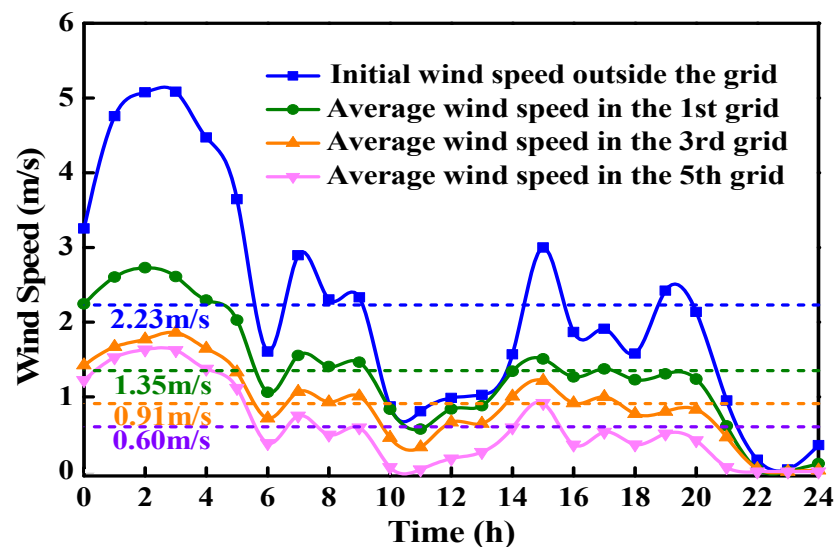


Figure 23. All-day near-surface wind speed.

According to the all-day near-surface wind speed data at the project point (Figure 23), the initial wind speed outside the grid and the average wind speed in the first, third, and fifth grids were 2.23, 1.35, 0.91, and 0.60 m/s, respectively. As the grid was laid deeper, the wind speed decreased step by step, indicating that the checkerboard sand barrier could gradually reduce the sand-carrying capacity of the wind such that the sand particles were far away from the rail and fell into the sand barrier grid, fixing the sand. After a certain period, the checkerboard sand barrier had a complete structure and gradually began to accumulate sand in the grid (Figure 24), indicating that the sand barrier system can adapt to harsh environments. The concept of “sand control with sand” could be confirmed, with the potential application in engineering.



Figure 24. Sand-fixing effect of the checkerboard sand barrier.

5.3. Sand-Resisting-Sand Fixing System

Using the sand-fixing board prepared with fiber-reinforced aeolian sand is a viable approach. To avoid wind-sand disasters, it is necessary to build upright hanging board sand barriers along the railway to achieve sand resistance. Such barriers have higher requirements for the mechanical properties of the sand-fixing board between columns. Insufficient flexural mechanical properties during the hoisting process of the board will cause the destruction of the sand barrier structure. It is necessary to add fiber cloth to the aeolian sand cement mortar while adding fibers (Figure 25) and to apply a prestress to the fiber cloth to meet the requirements of the upright sand barrier structure on the mechanical properties of the sand-fixing board. The prestressed fiber mesh cloth was laid in layers in the middle of the board, as shown in Figure 26. The maximum prestress applied using

different specifications of the mesh cloth was 9–35 N/mm, that is, the maximum prestress of 0.92–3.57 kg/mm width of the fiber mesh cloth could be applied. The application of a prestress made the interior of the sand-fixing board more compact and solid, which increased the overall mechanical strength of the board.

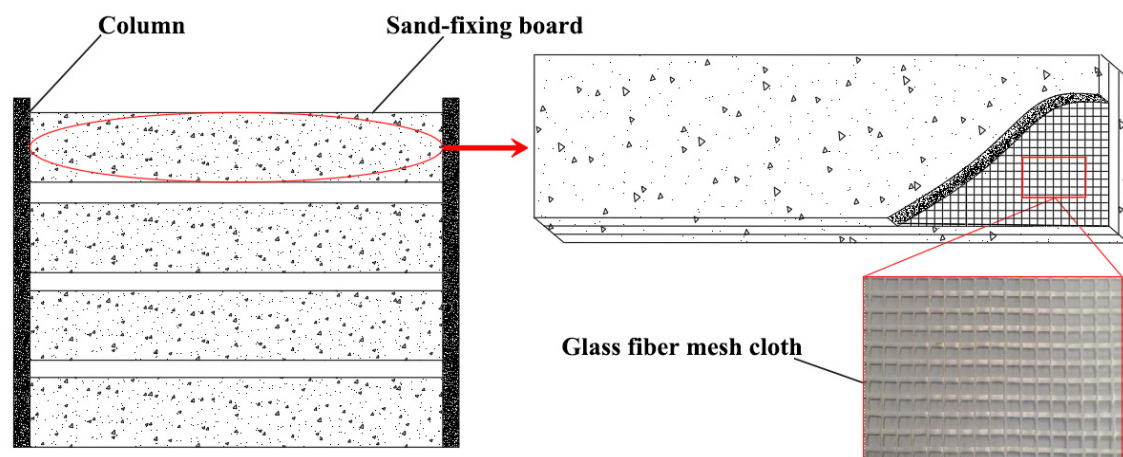


Figure 25. Schematic diagram of the structure.

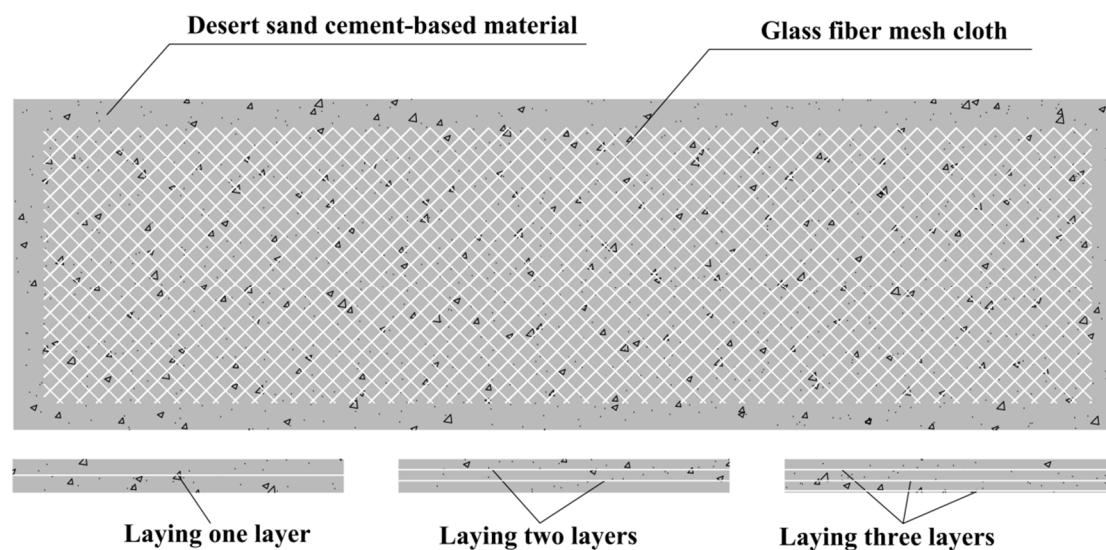


Figure 26. Schematic diagram of the position distribution of the glass fiber grid cloth.

The upright hanging board sand barrier and the checkerboard sand barrier together composed the sand-resisting-sand fixing engineering system along the railway, which was applied to the medium and high-wind-energy areas (Figure 27). First, the upright hanging board sand barrier was set in the direction of the sand flow as the first barrier, as shown in Figure 27a,b. They changed the local airflow field, reduced the near-surface wind speed, and greatly weakened the wind-carrying capacity. At the same time, the sand barrier itself resisted sand particles in the form of obstacles. Second, the checkerboard sand barrier was set as the second barrier, as shown in Figure 27c–e. At this time, the kinetic energy of the sand particles passing through the upright hanging board sand barrier was greatly reduced. After several layers of checkerboards, the sand particles settled into the grid, where they were fixed. This sand-resisting-sand fixing engineering system could give full play to the characteristics of in situ materials in severely damaged areas where the environment is harsh and materials are scarce. It can not only greatly reduce the project costs, but

also facilitates the rational use of resources, meets the requirements of ecologically sound construction methods, and can achieve the effect of “sand control with sand.”

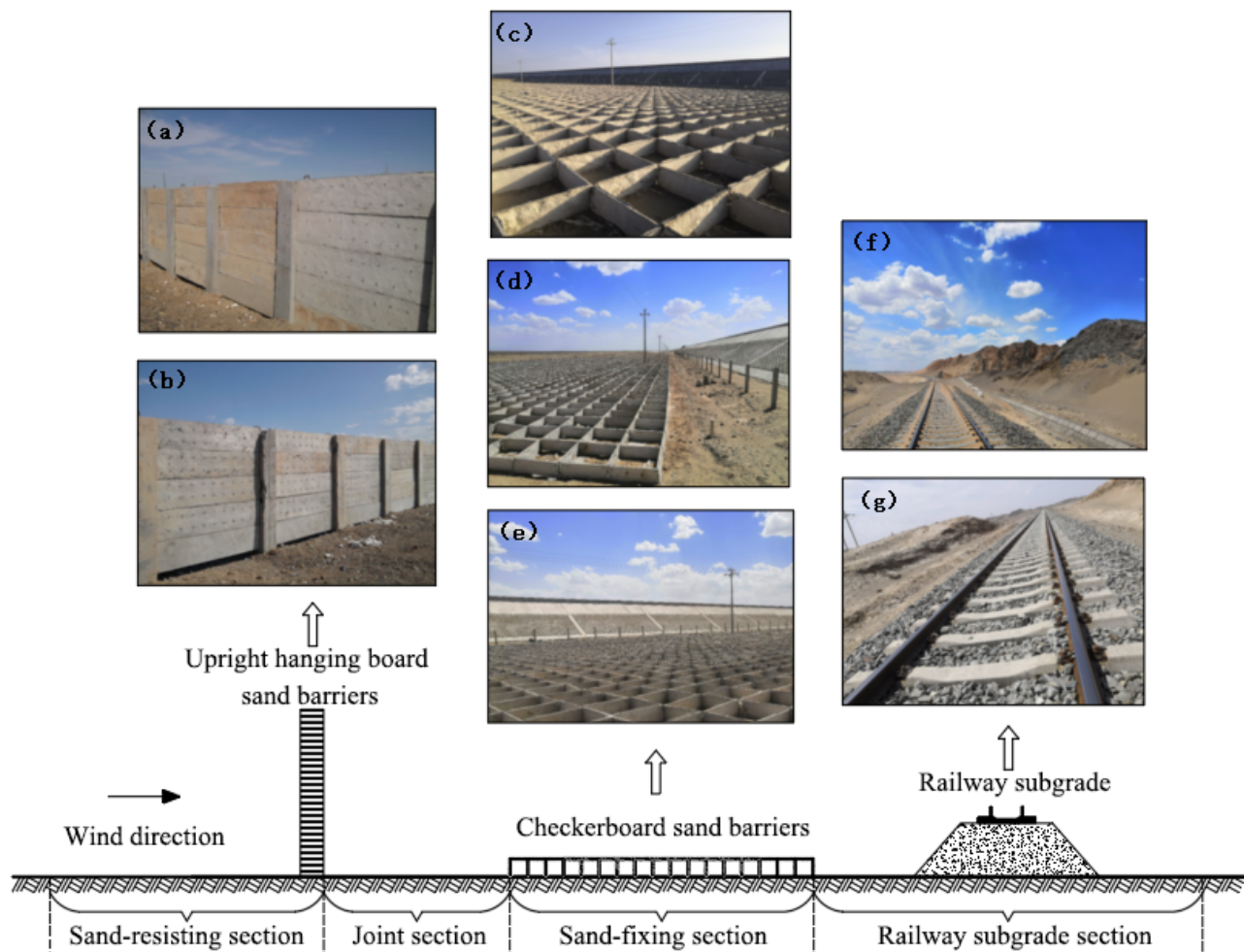


Figure 27. Sand-resisting-sand fixing engineering system along the railway line: (a,b) upright hanging board sand barriers; (c–e) checkerboard sand barriers; (f,g) railway subgrade.

6. Conclusions

According to an indoor test and field observations, the enhancement effect of fiber (cloth) on the performance of the sand-fixing board and the practical effects of the sand control project were analyzed; the main conclusions that were obtained are as follows:

- (1) Against the background of the lack of raw materials and high transportation costs for the railway sand control project in the uninhabited area of the Gobi Desert, a new type of sand-fixing board was prepared using fiber-modified aeolian sand and applied to the checkerboard sand barrier. It could increase the surface roughness to effectively reduce near-surface wind speed and the sand-carrying capacity of the wind. After long-term use, sand accumulation in the checkerboard sand barrier was obvious, and the engineering structure was complete. The scientific concept of “sand control with sand” was therefore put forward.
- (2) The mechanical strength of the sand-fixing board had different degrees of improvement with the addition of fiber. With the increase in fiber content and length, the overall strength of the board showed an upward trend. When the fiber content was 0.5% and the fiber length was 19 mm, the compressive strength of the sand-fixing board reached 20.03 MPa and the flexural strength reached 3.22 MPa after 28 days.

- Compared with the control group, the compressive strength and flexural strength increased by 2.15 and 0.59 times, respectively.
- (3) The apparent morphology of the sand-fixing board was gradually destroyed as the number of freeze–thaw cycles increased. When the numbers of freeze–thaw cycles were 0, 25, 50, and 75, the degree of damage was a complete structure (no freezing damage), slag on the surface and the corner of the mortar falling off (slight freezing damage), the surface layer falling off in a large area with obvious mass loss (moderate freezing damage), completely exposed internal fiber and a soft surface with obvious cracks and pores inside the structure (severe freezing damage). With the increase in the number of freeze–thaw cycles, the improvement in the mass loss rate of the sand-fixing board by the fiber became more obvious. After 75 freeze–thaw cycles, the mass loss rate of most boards did not exceed 5%, with a reduction of more than 60%.
 - (4) To avoid dry shrinkage cracking and an uneven fiber dispersion during the on-site production of the sand-fixing board, a complete set of fiber-reinforced sand-fixing board construction techniques can be summarized as follows: weighing, feeding sequencing, stirring, die filling, curing, and splicing. This can be used to guide on-site construction and has a practical reference value for the application of field projects.

Author Contributions: Conceptualization, B.D. and J.C.; methodology, J.C. and D.X.; software, D.X. and X.W.; validation, L.G., D.L. and Z.L.; formal analysis, B.M.; writing—original draft preparation, B.D. and B.M.; writing—review and editing, J.C. and L.G. All authors have read and agreed to the published version of the manuscript.

Funding: This research was funded by the Major Program of Science and Technology of Xinjiang Production and Construction Corps (2020AA002), National Natural Science Foundation of China (52168065), and the Program of Young and Middle-Aged Science and Technology Innovation Leading Talents of Xinjiang Production and Construction Corps (2019CB023).

Data Availability Statement: Not applicable.

Acknowledgments: The support from the College of Water Resources and Architectural Engineering at Shihezi University, China, is gratefully acknowledged. The authors also thank the reviewers and editors who helped to improve the quality of this paper.

Conflicts of Interest: The authors declare that they have no conflict of interest.

References

1. DeJong, J.T.; Fritzsche, M.B.; Nusslein, K. Microbially induced cementation to control sand response to undrained shear. *J. Geotech. Geoenviron. Eng.* **2006**, *132*, 1381–1392. [[CrossRef](#)]
2. Zhao, W.Z.; Hu, G.L.; Zhang, Z.H.; He, Z.B. Shielding effect of oasis-protection systems composed of various forms of wind break on sand fixation in an arid region: A case study in the Hexi Corridor, northwest China. *Ecol. Eng.* **2008**, *33*, 119–125. [[CrossRef](#)]
3. Liu, J.; Shi, B.; Lu, Y.; Jiang, H.; Huang, H.; Wang, G.; Kamai, T. Effectiveness of a new organic polymer sand-fixing agent on sand fixation. *Environ. Earth Sci.* **2012**, *65*, 589–595. [[CrossRef](#)]
4. Ju, Y.F.; Qiu, M.X.; Zhu, J.K.; Zhang, J.M.; Zhou, Y. Advances in sand-fixing material research in China and the application prospect. *J. Arid Land Resour. Environ.* **2019**, *33*, 138–144. [[CrossRef](#)]
5. Qu, H.J.; Zu, R.P.; Zhang, K.; Fang, H.Y. Field observations on the protective effect of semi-buried checkerboard sand barriers. *Geomorphology* **2007**, *88*, 193–200. [[CrossRef](#)]
6. Wang, T.; Qu, J.J.; Niu, Q.H. Comparative study of the shelter efficacy of straw checkerboard barriers and rocky checkerboard barriers in a wind tunnel. *Aeolian Res.* **2020**, *43*, 100575. [[CrossRef](#)]
7. Azoogh, L.; Moghadam, B.K.; Jafari, S. Interaction of petroleum mulching, vegetation restoration and dust fallout on the conditions of sand dunes in southwest of Iran. *Aeolian Res.* **2018**, *32*, 124–132. [[CrossRef](#)]
8. Wang, Y.M. Study on mechanism of chemical desert control. *J. Catastrophol.* **2008**, *23*, 32–35, (in Chinese with English abstract). [[CrossRef](#)]
9. Meng, X.; Peng, G.; Liu, B.L.; Wang, B.; Chen, H.L.; Luo, R.; Dong, Z.B.; Li, Y.; Zhang, B.; Luo, L.H. Synthesis and Sand-Fixing Property of Cationic Poly(Vinyl Acetate-Butyl Acrylate-DMC) Copolymer Emulsions. *Polym.-Plast. Technol. Eng.* **2013**, *52*, 931–939. [[CrossRef](#)]
10. Dang, X.G.; Chen, H.; Shan, Z.H. Preparation and characterization of poly(acrylic acid)-corn starch blend for use as chemical sand-fixing materials. *Mater. Res. Express* **2017**, *4*, 075506. [[CrossRef](#)]

11. Gong, W.; Li, M.L.; Zang, Y.X.; Xie, H.; Liu, B.L.; Chen, H.L. The synthesis of salt-resistant emulsion and its application in ecological sand-fixing of high salt-affected sandy land. *Plast. Rubber Compos.* **2017**, *46*, 163–172. [[CrossRef](#)]
12. Liu, X.; Tie, S. Weather resistance of $\text{CaSO}_4 \cdot 1/2\text{H}_2\text{O}$ -based sand-fixation material. *Int. J. Mod. Phys. B* **2017**, *31*, 1744084. [[CrossRef](#)]
13. Xie, H.; Liu, B.L.; Chen, H.L.; Xu, Q. Inner relationship between the damping property and the sand-fixing durability of polymer materials. *J. Appl. Polym. Sci.* **2019**, *136*, 47208. [[CrossRef](#)]
14. DeJong, J.T.; Mortensen, B.M.; Martinez, B.C.; Nelson, D.C. Bio-mediated soil improvement. *Ecol. Eng.* **2010**, *36*, 197–210. [[CrossRef](#)]
15. Van Paassen, L.A.; Ghose, R.; van der Linden, T.J.M.; van der Star, W.R.L.; van Loosdrecht, M.C.M. Quantifying Biomediated Ground Improvement by Ureolysis: Large-Scale BiogROUT Experiment. *J. Geotech. Geoenviron. Eng.* **2010**, *136*, 1721–1728. [[CrossRef](#)]
16. Burbank, M.B.; Weaver, T.J.; Green, T.L.; Williams, B.C.; Crawford, R.L. Precipitation of Calcite by Indigenous Microorganisms to Strengthen Liquefiable Soils. *Geomicrobiol. J.* **2011**, *28*, 301–312. [[CrossRef](#)]
17. Fujita, Y.; Taylor, J.L.; Wendt, L.M.; Reed, D.W.; Smith, R.W. Evaluating the potential of native ureolytic microbes to remediate a ^{90}Sr contaminated environment. *Environ. Sci. Technol.* **2010**, *44*, 7652–7658. [[CrossRef](#)] [[PubMed](#)]
18. Okwadha, G.D.O.; Li, J. Biocontainment of polychlorinated biphenyls (PCBs) on flat concrete surfaces by microbial carbonate precipitation. *J. Environ. Manag.* **2011**, *92*, 2860–2864. [[CrossRef](#)]
19. Rusu, C.; Cheng, X.H.; Li, M. Biological Clogging in Tangshan Sand Columns under Salt water Intrusion by *Sporosarcina Pasteurii*. *Adv. Mater. Res.-Switz.* **2011**, *250–253*, 2040–2046. [[CrossRef](#)]
20. Yan, W.L.; Wu, G.; Dong, Z.Q. Optimization of the mix proportion for desert sand concrete based on a statistical model. *Constr. Build. Mater.* **2019**, *226*, 469–482. [[CrossRef](#)]
21. Cai, H.; Liao, T.C.; Ren, S.Q.; Li, S.G.; Huo, R.K.; Yuan, J.; Yang, W.C. Predicting the compressive strength of desert sand concrete using ANN: PSO and its application in tunnel. *Adv. Civ. Eng.* **2020**, *2020*, 8875922. [[CrossRef](#)]
22. Liu, H.F.; Chen, X.L.; Che, J.L.; Liu, N.; Zhang, M.H. Mechanical performances of concrete produced with desert sand after elevated temperature. *Int. J. Concr. Struct. Mater.* **2020**, *14*, 26. [[CrossRef](#)]
23. Li, X.A.; Zheng, H.F.; Li, X.X.; Ye, W.J. Test on the mortar mix ratio with aeolian sand of mu us desert. *Adv. Mater. Res.* **2011**, *152–153*, 892–896. [[CrossRef](#)]
24. Benabed, B.; Azzouz, L.; Kadri, E.; Kenai, S.; Belaidi, A.S.E. Effect of fine aggregate replacement with desert dune sand on fresh properties and strength of self-compacting mortars. *J. Adhes. Sci. Technol.* **2014**, *28*, 2182–2195. [[CrossRef](#)]
25. Al-Lebban, M.F.; Khazaly, A.I.; Shabbar, R.; Jabal, Q.A.; Al Asadi, L.A.R. Effect of polypropylene fibers on some mechanical properties of concrete and durability against freezing and thawing cycles. *Key Eng. Mater.* **2021**, *895*, 130–138. [[CrossRef](#)]
26. Zhang, P.; Han, X.; Zheng, Y.; Wan, J.; Hui, D. Effect of PVA fiber on mechanical properties of fly ash-based geopolymer concrete. *Rev. Adv. Mater. Sci.* **2021**, *60*, 418–437. [[CrossRef](#)]
27. Zhang, P.; Gao, Z.; Wang, J.; Wang, K. Numerical modeling of rebar-matrix bond behaviors of nano-SiO₂ and PVA fiber reinforced geopolymer composites. *Ceram. Int.* **2021**, *47*, 11727–11737. [[CrossRef](#)]
28. Zhang, P.; Wang, J.; Li, Q.; Wan, J.; Ling, Y. Mechanical and fracture properties of steel fiber-reinforced geopolymer concrete. *Sci. Eng. Compos. Mater.* **2021**, *28*, 299–313. [[CrossRef](#)]
29. Zhang, P.; Li, Q.F. Effect of polypropylene fiber on durability of concrete composite containing fly ash and silica fume. *Compos. Part B Eng.* **2013**, *45*, 1587–1594. [[CrossRef](#)]
30. Patel, V.; Singh, B.; Ojha, P.N.; Adhikari, S. Mechanical properties of polypropylene fiber reinforced concrete under elevated temperature. *J. Archit. Environ. Struct. Eng. Res.* **2021**, *4*, 45–53. [[CrossRef](#)]
31. Murali, G.; Abid, S.R.; Karthikeyan, K.; Haridharan, M.K.; Amran, M.; Siva, A. Low-velocity impact response of novel prepacked expanded clay aggregate fibrous concrete produced with carbon nano tube, glass fiber mesh and steel fiber. *Constr. Build. Mater.* **2021**, *284*, 122749. [[CrossRef](#)]
32. Sucharda, O.; Konecny, P.; Kubosek, J.; Ponikiewski, T.; Done, P. Finite Element Modelling and Identification of the Material Properties of Fibre Concrete. *Procedia Eng.* **2015**, *109*, 234–239. [[CrossRef](#)]